THE JOURNAL OF PHYSICAL CHEMISTRY LETTERS
A JOURNAL OF THE AMERICAN CHEMICAL SOCIETY

pubs.acs.org/JPCL Letter

Gas-Phase Preparation of Subvalent Germanium Monoxide (GeO, $X^1\Sigma^+$) via Non-Adiabatic Reaction Dynamics in the Exit Channel

Chao He, Shane J. Goettl, Zhenghai Yang, Ralf I. Kaiser,* Anatoliy A. Nikolayev, Valeriy N. Azyazov, and Alexander M. Mebel*

Cite This: *J. Phys. Chem. Lett.* 2022, 13, 4589−4597 Read Online

ACCESS | Metrics & More | Article Recommendations | Supporting Information

ABSTRACT: The subvalent germanium monoxide (GeO, $X^1\Sigma^+$) molecule has been prepared via the elementary reaction of atomic germanium (Ge, ^3P_j) and molecular oxygen (O_2, $X^3\Sigma_g^-$) with each reactant in its electronic ground state by means of single-collision conditions. The merging of electronic structure calculations with crossed beam experiments suggests that the formation of germanium monoxide (GeO, $X^1\Sigma^+$) commences on the singlet surface through unimolecular decomposition of a linear singlet collision complex (GeOO, **i1**, $C_{\infty v}$, $^1\Sigma^+$) via intersystem crossing (ISC) yielding nearly exclusively germanium monoxide (GeO, $X^1\Sigma^+$) along with atomic oxygen in its electronic ground state [**p1**, $O(^3P)$]. These results provide a sophisticated reaction mechanism of the germanium−oxygen system and demonstrate the efficient "heavy atom effect" of germanium in ISC yielding (nearly) exclusive singlet germanium monoxide and triplet atomic oxygen compared to similar systems (carbon dioxide and dinitrogen monoxide), in which non-adiabatic reaction dynamics represent only minor channels.

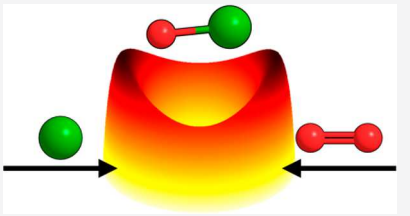

As early as in 1886, the chemist Clement Winkler initiated the pioneering report of the main group XIV element germanium (Ge).[1,2] The preparation and properties of subvalent germanium(II) compounds along with their isovalent carbon (C) and silicon (Si) analogues have attracted the attention of the physical inorganic, synthetic, and computational chemistry communities from the perspective of chemical bonding and electronic structure theory.[3−11] From carbon to germanium, the electronic structures of the dihydrides change dramatically (Scheme 1, **1**−**6**). Whereas methylene (CH_2, X^3B_1) has a triplet electronic ground state with a singlet−triplet splitting to the a^1A_1 state of 35.6−37.7 kJ mol^{-1},[12,13] the situation is reversed for silylene (SiH_2) and germylene (GeH_2) with X^1A_1 determined as the electronic ground state and a^3B_1 confirmed as the first excited electronic state. The singlet−triplet splitting rises from 79.5−87.9 kJ mol^{-1} in silylene[14−20] to 100−105 kJ mol^{-1} in germylene (GeH_2).[21] This finding has been discussed on the basis of distinct sizes of the valence orbitals of carbon versus silicon and germanium (the larger size of the valence orbitals of silicon and germanium leading to an inefficient hybridization of the s and p orbitals in silicon and germanium and hence stabilization of the singlet versus triplet state in silylene and germylene); this conclusion is also evident from the H−E−H (E = C, Si, or Ge) angles in the electronic ground states, which are reduced from 129.8° (CH_2, X^3B_1) to 93.4° (SiH_2, X^1A_1) and 92.3° (GeH_2, X^1A_1) (Scheme 1).[22] The diminished reactivity of germylene (GeH_2)[23] compared to those of their methylene (CH_2)[24−28] and silylene (SiH_2) analogues[29−31] led to the successful synthesis and characterization of subvalent germanium(II) compounds such as the germanium dichloride adduct $GeCl_2$ (benzthiazole),[3] the acyclic germylene diamide $[(Me_3Si)_2N]_2Ge$,[4,5] and the germanium analogue of Arduengo's carbene (*t*-BuNCHCHN*t*-Bu)Ge.[6−8]

The growing interest in the (in)organic germanium(II) chemistry also re-energized extensive research of the chemical bonding of binary oxides of main group XIV elements. In carbon monoxide (CO, **7**), two π bonds and one σ bond essentially form a C≡O bond.[32,33] Whereas carbon monoxide is a gas at 293 K, gas-phase silicon monoxide (SiO, **8**), which was first reported by Mabery,[34] is inherently unstable and reacts through disproportionation to afford amorphous silicon and silicon dioxide (SiO_2) clusters.[35,36] The divalent germanium monoxide (GeO, **9**)[37] was first discovered by Winkler.[1] From carbon to silicon and germanium, the bond lengths increase from 1.128 Å to 1.512 and 1.617 Å, respectively. Germanium monoxide has emerged as a key reactive intermediate in the fabrication of integrated optics[38] and silicon−germanium alloy-based microelectronic devices due to enhanced electron and hole mobilities compared to those of silicon.[39,40] Germanium monoxide has been characterized spectroscopically both experimentally[41−43] and theoretically[44−46] by exploiting ultraviolet−visible spectroscopy in gas discharges of germanium tetrachloride ($GeCl_4$) vapor

Received: March 9, 2022
Accepted: May 16, 2022

https://doi.org/10.1021/acs.jpclett.2c00706
J. Phys. Chem. Lett. 2022, 13, 4589−4597

Scheme 1. Molecular Structures of Divalent Hydrides Methylene (CH_2), Silylene (SiH_2), and Germylene (GeH_2) as Well as the Oxides Carbon Monoxide (CO), Silicon Monoxide (SiO), and Germanium Monoxide (GeO)[a]

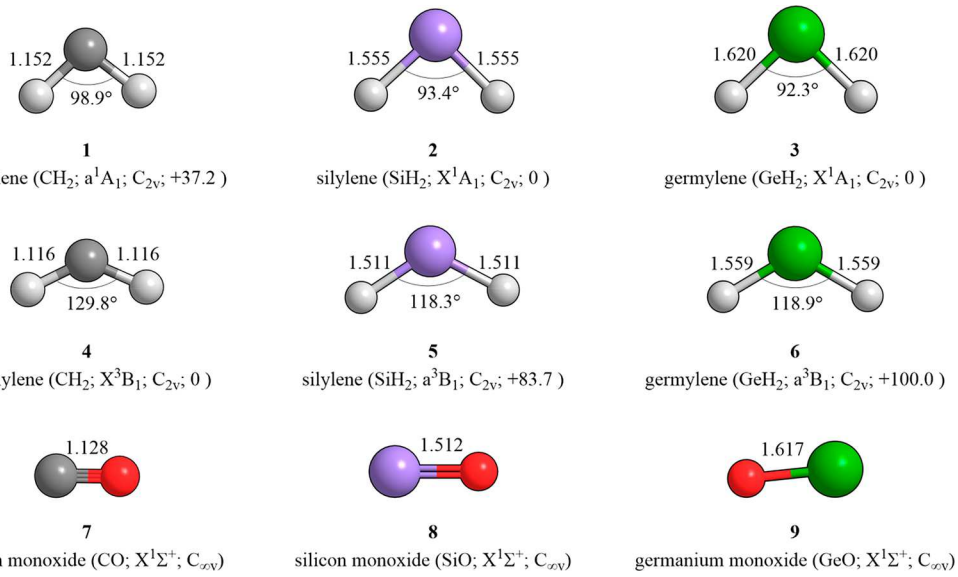

[a]The corresponding relative energies (kilojoules per mole) and bond distances (angstroms) are also included. The atoms are colored black (carbon), purple (silicon), green (germanium), red (oxygen), and gray (hydrogen).

and oxygen (O_2).[47,42,48,49] Trickle and co-workers extended this range to the vacuum ultraviolet region in an inductively heated furnace, thus characterizing the $X^2\Sigma^+$, $A^2\Pi$, and $B^2\Sigma^+$ states.[50]

However, whereas subvalent germanium monoxide has been successfully characterized spectroscopically, no route for preparing divalent germanium monoxide (GeO, **9**) in a directed synthesis has been developed. At this point, we conducted the first gas-phase preparation of germanium monoxide (GeO, **9**, $X^1\Sigma^+$) through the reaction of germanium atoms (Ge, ^3P_j) with molecular oxygen (O_2, $X^3\Sigma_g^-$) with each reactant in its electronic ground state via the technique of crossed molecular beams.[51,52] The most fundamental and microscopic level studies fused with electronic structure calculations offer an exceptional glance into the underlying reaction dynamics through which highly reactive germanium oxides like germanium oxide (GeO, **9**, $X^1\Sigma^+$) may be prepared via a bimolecular reaction between the simplest germanium-bearing species (Ge, ^3P_j) and the prototype oxidant (O_2, $X^3\Sigma_g^-$) under single-collision conditions involving unconventional non-adiabatic reaction dynamics in the exit channel. This system is also of fundamental interest to the reaction dynamics community as a benchmark of triatomic systems such as the reactions of hydrogen (H, ^2S),[53−55] chlorine, (Cl, ^2P),[56−60] fluorine (F, ^2P),[61−65] carbon (C, ^1D),[66,67] nitrogen (N, ^2D),[68−71] oxygen (O, ^1D),[72,73] and sulfur (S, $^3P/^1D$)[74−76] atoms with molecular hydrogen (H_2, $X^1\Sigma_g^+$, $v = 0, 1$) with the reaction dynamics of triatomic systems involving the "heavy" main group XIV element germanium being elusive until now.

The elementary gas-phase bimolecular reaction of atomic germanium (Ge, ^3P_j) with molecular oxygen (O_2, $X^3\Sigma_g^-$) with each reactant in its electronic ground state was investigated under single-collision conditions utilizing a crossed molecular beam machine (Methods). The branching ratios of the natural isotope abundances of germanium ^{70}Ge, ^{72}Ge, ^{73}Ge, ^{74}Ge, and ^{76}Ge are 20.4%, 27.3%, 7.7%, 36.7%, and 7.8%, respectively. Therefore, the reactive scattering signals were observed at m/z 86, 88, 89, 90, and 92, respectively. No adducts ($^{70}Ge^{32}O_2^+$, m/z 102; $^{72}Ge^{32}O_2^+$, m/z 104; $^{73}Ge^{32}O_2^+$, m/z 105; $^{74}Ge^{32}O_2^+$, m/z 106; $^{76}Ge^{32}O_2^+$, m/z 108) were detectable. These raw data alone demonstrate a single reaction channel via the emission of atomic oxygen (16 amu) and formation of germanium monoxide (hereafter GeO) ($^{70}Ge^{16}O^+$, m/z 86; $^{72}Ge^{16}O^+$, m/z 88; $^{73}Ge^{16}O^+$, m/z 89; $^{74}Ge^{16}O^+$, m/z 90; $^{76}Ge^{16}O^+$, m/z 92) (reaction 1). The corresponding TOF spectra and the laboratory angular distribution (LAD) were collected at the best signal-to-noise ratio at m/z 90 (Figure 1). The LAD is rather broad and spans the complete range of the rotatable detector from at least 9.25° to 64.25°.

$$^{74}Ge(^3P;\ 74\ amu) + {}^{32}O_2\left(X^3\Sigma_g^-;\ 32\ amu\right) \rightarrow {}^{74}Ge^{16}O(X^1\Sigma^+;\ 90\ amu) + {}^{16}O(^3P;\ 16\ amu) \quad (1a)$$

$$^{74}Ge(^3P;\ 74\ amu) + {}^{32}O_2\left(X^3\Sigma_g^-;\ 32\ amu\right) \rightarrow {}^{74}Ge^{16}O(X^1\Sigma^+;\ 90\ amu) + {}^{16}O(^1D;\ 16\ amu) \quad (1b)$$

The aforementioned experimental results support the formation of the germanium monoxide (GeO, $X^1\Sigma^+$) along with atomic oxygen under single-collision conditions. To further illuminate the underlying reaction mechanism(s) accompanied by the potential involvement of intersystem crossing (ISC), excited state surfaces, and non-adiabatic reaction dynamics, a transformation of the laboratory data from the laboratory reference frame into the center-of-mass reference frame is accomplished. Figure 2 shows the corresponding center-of-mass translational energy $P(E_T)$ and angular $T(\theta)$ flux distributions. Within the margin of error, the TOFs and LAD (Figure 1) can be duplicated well via a single-channel fit, that is, the reaction ^{74}Ge (^3P_j; 74 amu) + $^{32}O_2$ ($X^3\Sigma_g^-$; 32 amu) → $^{74}Ge^{16}O$ ($X^1\Sigma^+$; 90 amu) + ^{16}O (^3P; 16 amu) (reaction 1a) (Figure 1). In detail, for molecules born without internal excitation, the relation $E_{max} = E_C - \Delta_r G$ is used to describe the conservation of energy among the

https://doi.org/10.1021/acs.jpclett.2c00706
J. Phys. Chem. Lett. 2022, 13, 4589−4597

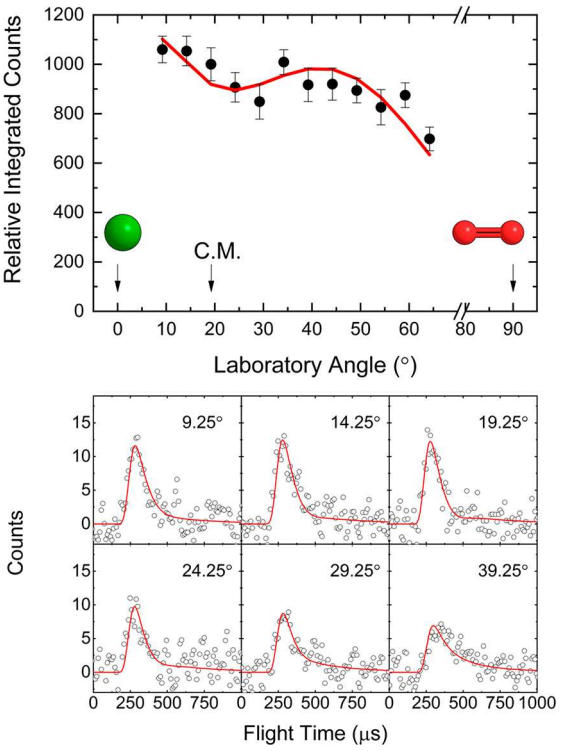

Figure 1. Laboratory angular distribution (top) and time-of-flight (TOF) spectra (bottom) recorded at m/z 90 for the reaction of a germanium (^{74}Ge, ^3P_j) atom with molecular oxygen (O_2, $X^3\Sigma_g^-$). The experimental data are shown as black circles. The red lines depict the best fits.

maximum translational energy E_{max} of the center-of-mass translational energy distribution $P(E_T)$, the collision energy (E_C), and the reaction energy (Δ_rG). E_{max} can be easily derived from $P(E_T)$, which terminates at 184 ± 19 kJ mol^{-1} (Figure 2A). Therefore, the reaction is exoergic along with a reaction energy of 167 ± 19 kJ mol^{-1}. Moreover, the $P(E_T)$ distribution peaks at 88 ± 9 kJ mol^{-1}, indicating a tight exit transition state yielding germanium monoxide along with an oxygen atom.[77] The average translational energy of the products was derived to be 90 ± 9 kJ mol^{-1}, suggesting that nearly half of the total available energy (49 ± 5%) is channeled into the translational degrees of freedom of the products. The center-of-mass angular distribution $T(\theta)$ can provide additional information about the reaction dynamics (Figure 2B). First, $T(\theta)$ is forward−backward symmetric and exhibits non-zero intensity over the complete angular range from 0° to 180°; this proposes indirect scattering dynamics via long-lived complex formation and hence the existence of bound GeO_2 intermediate(s). Furthermore, the distribution minimum at 90° reveals geometrical limitations and an emission of the oxygen atom nearly perpendicular to the total angular momentum vector within the rotational plane of the fragmenting complex(es).[78,79] These findings are also summarized in the flux contour map, which depicts the flux intensity of the reactive scattering products as a function of the product velocity (u) and center-of-mass scattering angle (θ), providing detailed information about the reactive scattering process (Figure 2C).[77]

The underlying chemical dynamics and mechanism(s) of $Ge(^3P_j)$−$O_2(X^3\Sigma_g^-)$ reaction can be unlocked through the combination of the laboratory data with electronic structure calculations (Figure 3 and Table S2). The existence of two atomic oxygen loss channels (**p1** and **p2**) on the triplet and singlet surface, respectively, is revealed by the electronic structure calculations. These lead to germanium monoxide (GeO, $X^1\Sigma^+$) along with ground state atomic oxygen [**p1**, $O(^3P)$; Δ_rG = −170 ± 5 kJ mol^{-1}; reaction 1a] and electronically excited singlet oxygen [**p2**, $O(^1D)$; Δ_rG = 20 ± 5 kJ mol^{-1}; reaction 1b]. The computed reaction energy to form germanium monoxide (GeO, $X^1\Sigma^+$) and ground state atomic oxygen matches well with the reaction energy of −164 ± 10 kJ mol^{-1} derived by Doering et al.[80] and Schnedler et al.[81] A comparison of the computed reaction energies (for **p1**, Δ_rG = −170 ± 5 kJ mol^{-1}; for **p2**, Δ_rG = 20 ± 5 kJ mol^{-1}) with the experimentally deduced value from the crossed beam study (Δ_rG = −167 ± 19 kJ mol^{-1}) suggests that germanium monoxide (GeO, $X^1\Sigma^+$) along with ground state atomic oxygen [$O(^3P)$] (**p1**) is formed. It is worth noting that the reaction energies (Figure 3) are computed for germanium atoms in their ^3P_j (j = 0) state. The presence of $^3P_0$, $^3P_1$, and $^3P_2$ of the germanium beam was confirmed by laser-induced fluorescence (LIF) characterization.[82] Compared with $Ge(^3P_0)$, $Ge(^3P_1)$ and $Ge(^3P_2)$ are 6.7 and 16.9 kJ mol^{-1} higher in energy, respectively. This would change the reaction energies from −170 ± 5 to −177 ± 5 kJ mol^{-1} (j = 1) and −187 ± 5 kJ mol^{-1} (j = 2) for **p1** and from 20 ± 5 to 13 ± 5 kJ mol^{-1} (j = 1) and 3 ± 5 kJ mol^{-1} (j = 2) for **p2**. Therefore, within the margin of error, the thermodynamically most stable product channel (**p1**) may be the result of the reaction of germanium in the ^3P_j (j = 0, 1, and 2) states. Considering the experimental and computational error limits, the channel to **p2** might be concealed in the low-energy part of the center-of-mass translational energy distribution with fractions of 5 ± 3%. In summary, the data support the dominant formation of germanium monoxide (GeO, $X^1\Sigma^+$) along with atomic oxygen [$O(^3P)$] in its electronic ground state via single-collision conditions on the triplet surface in the gas phase with minor amounts of the reactive scattering signal perhaps originating from the singlet surface.

Which is the dominating reaction mechanism to germanium monoxide (GeO, $X^1\Sigma^+$) and ground state atomic oxygen [$O(^3P)$]? For the $Ge(^3P_j)$−$O_2(^3\Sigma_g^-)$ reaction, both reactants are in their triplet electronic ground states, along with the singlet and/or triplet electronic states of the germanium monoxide (GeO, $X^1\Sigma^+$) and atomic oxygen [$O(^1D/^3P)$]. Therefore, the triplet and singlet GeO_2 surfaces have to be explored. The computations identified three singlet (**i1**, **i3**, and **i5**) and two triplet (**i2** and **i4**) GeO_2 intermediates, four transition states (**TS1**−**TS4**), and six singlet−triplet seams of crossings (**MSX1a**, **MSX1b**, and **MSX2**−**MSX5**). The reaction can be initiated via the addition of ground state germanium (Ge, ^3P) to one of the oxygen atoms of molecular oxygen without any barrier leading to a linear singlet (GeOO, **i1**, $C_{\infty v}$, $^1\Sigma^+$) and/or, via a tiny barrier of 5 kJ mol^{-1}, to form a bent triplet (GeOO, **i2**, C_s, $^3A''$) collision complex. On the triplet surface, the migration of the terminal oxygen atom to the germanium atom in **i2** yields a bent germanium dioxide (OGeO, **i4**, C_{2v}, $^3B_2$), which then undergoes a barrierless, unimolecular decomposition to germanium monoxide (GeO, $C_{\infty v}$, $X^1\Sigma^+$) along with ground state atomic oxygen [**p1**, $O(^3P)$]. On the singlet surface, ring closure in **i1** (GeOO, $C_{\infty v}$, $^1\Sigma^+$) accompanied by a second Ge−O bond formation results in a cyclic, triangular intermediate **i3** (OGeO, C_{2v}, $^1A_1$). Intermediate **i3** (OGeO, C_{2v}, $^1A_1$) can also be accessed from

https://doi.org/10.1021/acs.jpclett.2c00706
J. Phys. Chem. Lett. 2022, 13, 4589−4597

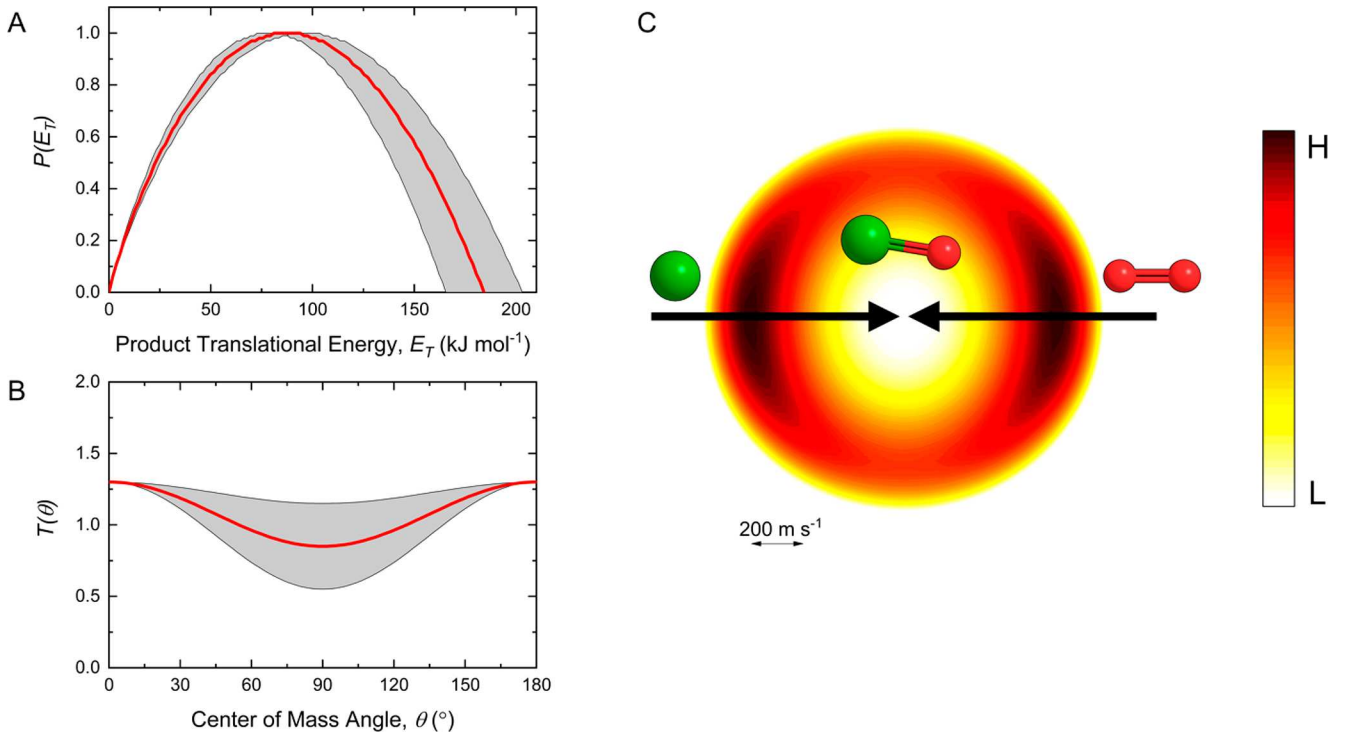

Figure 2. (A) CM translational energy flux distribution, (B) CM angular flux distribution, and (C) top view of the corresponding flux contour map leading to the formation of germanium monoxide (GeO, $X^1\Sigma^+$) and an oxygen atom (^{16}O, ^3P) in the reaction of atomic germanium (^{74}Ge, ^3P_j) with molecular oxygen (O_2, $X^3\Sigma_g^-$). The gray envelopes indicate the acceptable upper and lower error limits, while the red solid lines define the best fits. The flux contour map describes the flux intensity of the reactively scattered heavy products as a function of the CM scattering angle (θ) and product velocity (u). The flux intensity changes from high (H) to low (L) can be reflected in the color bar. The atoms are colored green (germanium) and red (oxygen).

the reactants in nearly zero-impact parameter collisions and isomerizes via ring opening to **i5** (OGeO, $D_{\infty h}$, $^1\Sigma_g^+$) via a transition state lying 91 kJ mol^{-1} above **i3**. Singlet germanium dioxide (OGeO, **i5**, $D_{\infty h}$, $^1\Sigma_g^+$) represents the global minimum of the GeO_2 potential energy surface. The product germanium monoxide (GeO, $X^1\Sigma^+$) along with electronically excited singlet oxygen [**p2**, O(^{1}D)] can be formed via emission of a terminal atomic oxygen in **i1** (GeOO, $C_{\infty v}$, $^1\Sigma^+$) and **i5** (OGeO, $D_{\infty h}$, $^1\Sigma_g^+$) without an exit barrier. To determine the possibility of ISC among the triplet and singlet surfaces, investigations were expanded to identify six minima on the seams of crossings (MSX) (**MSX1a**, **MSX1b**, and **MSX2**−**MSX5**). In energetic terms, two seams of crossings, **MSX1a** and **MSX1b**, are located nearby intermediate **i2** (GeOO, C_s, $^3A''$) and in the vicinity of the isomerization path of **i1** (GeOO, $C_{\infty v}$, $^1\Sigma^+$) to **i3** (OGeO, C_{2v}, $^1A_1$). Here, judging from the Ge−O−O angle, **MSX1a** is placed prior to passing transition state **TS1**, so that after the crossing, the system proceeds to **i1**. Alternatively, **MSX1b** is located after **TS1**, on the path toward **i3**. **MSX2** resides in the vicinity of the isomerization pathway of **i3** (OGeO, C_{2v}, $^1A_1$) to **i5** (OGeO, $D_{\infty h}$, $^1\Sigma_g^+$) and acts like atransition state connecting **i3** to **i4** (OGeO, C_{2v}, $^3B_2$). **MSX3**, which is 27 kJ mol^{-1} in energy below the separated reactants, links intermediate **i1** (GeOO, $C_{\infty v}$, $^1\Sigma^+$) to the products germanium monoxide (GeO, $X^1\Sigma^+$) plus ground state atomic oxygen [**p1**, O(^{3}P)]. **MSX4** lies on the dissociation pathway from **i3** to **p1** and is located 232 kJ mol^{-1} lower in energy compared with the initial reactants or 62 kJ mol^{-1} below product **p1**. Similarly, **MSX5** is positioned on the decomposition pathway of **i5** to **p1** and lies 174 and 4 kJ mol^{-1} lower in energy compared with the reactants and product, respectively. It means that the spin-forbidden dissociation of singlet intermediates **i3** and **i5** to the triplet product **p1** occurs via **MSX4** and **MSX5** without exit barriers. Interestingly, no direct oxygen atom abstraction pathway that connects the reactants to any products could be found on the triplet surface. A transition state search for this pathway was unsuccessful, and the potential energy scan for the germanium atom approach toward molecular oxygen showed a monotonic energy decrease with the system descending to the **i2** complex on the triplet PES after a small entrance barrier at **TS4** is overcome.

The aforementioned pathways are filtered further based upon the experimental results for $P(E_T)$ and $T(\theta)$. First, the peak of $P(E_T)$ at 88 ± 9 kJ mol^{-1} reveals a tight exit transition state leading to germanium monoxide (GeO, $X^1\Sigma^+$) along with atomic oxygen in its electronic ground state [**p1**, O(^{3}P)]. Considering the possible pathways, the unimolecular decomposition of **i1** through **MSX3**, which resides 143 kJ mol^{-1} above the separated products, can account for the experimentally predicted tight exit transition state. The **i4** → **p1** pathway can be likely excluded because the decomposition of **i4** involves a loose exit transition state, a feature that is not corroborated by our experiments. The same is true for the spin-forbidden **i3** → **p1** and **i5** → **p1** pathways. Second, $T(\theta)$ features a minimum at 90°; this finding reveals a dominating decomposition of the GeO_2 intermediate in which the oxygen atom is ejected nearly within the rotational plane of the fragmenting complex(es). Although our laboratory data cannot provide the rotational energy distribution of GeO, the experimentally derived $P(E_T)$ and $T(\theta)$ provide strong evidence of the involvement of the **i1** → **MSX3** → **p1** pathway in this system.

https://doi.org/10.1021/acs.jpclett.2c00706
J. Phys. Chem. Lett. 2022, 13, 4589−4597

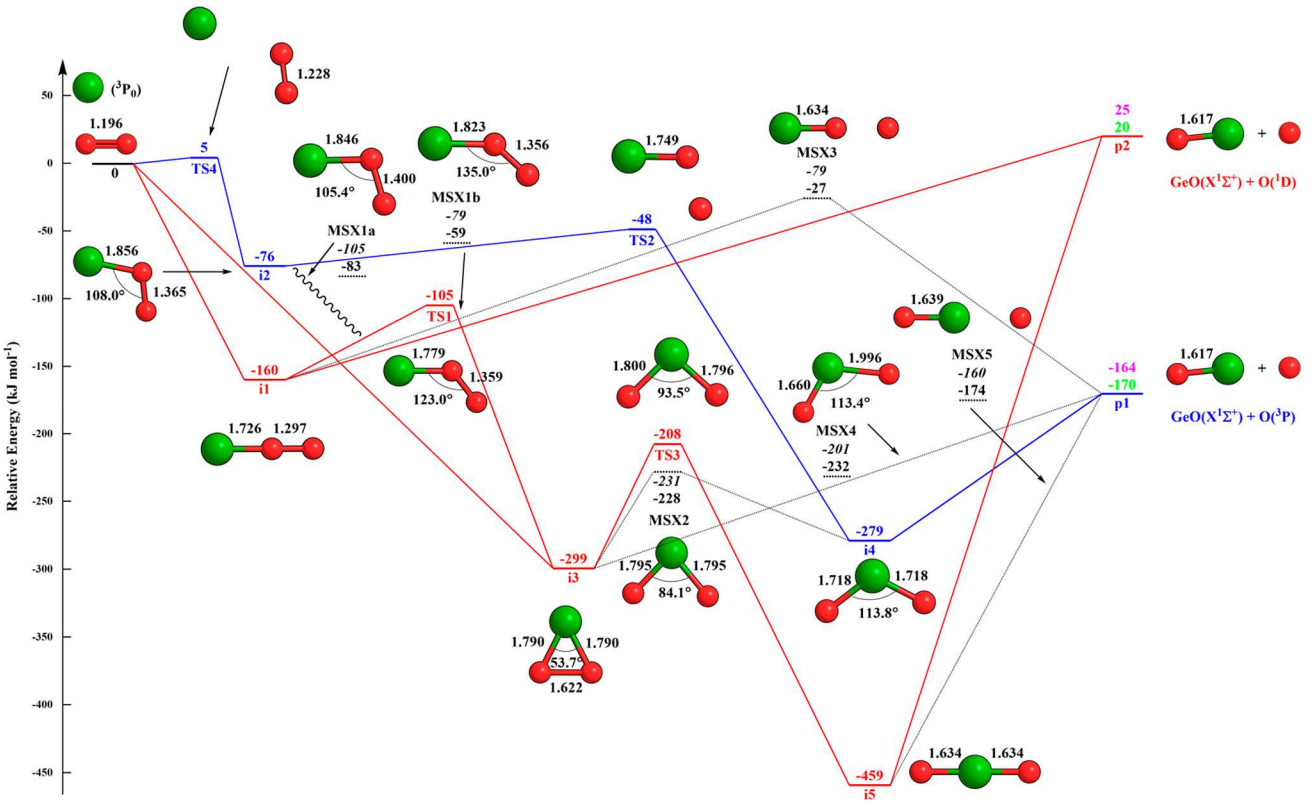

Figure 3. PES of the reaction of atomic germanium (Ge, ^3P_j) with oxygen (O_2, $X^3\Sigma_g^-$). The plain numbers colored red, blue, and black give the energies at the CASPT2(16,12)/aug-cc-pVQZ level of theory with ZPE, and those in italic for MSX refer to CASSCF(16,12)/x2c-SVPall-2c calculations. The reaction energies of the products are calculated using CCSD(T)/CBS(aug-cc-pVQZ,aug-cc-pVTZ)//ωb97xd/aug-cc-pVTZ (green) and via enthalpies of formation (pink), respectively. The geometries of MSXs are optimized at the CASSCF(16,12)/x2c-SVPall-2c level of theory, and their single-point energies are also recalculated at the CASPT2(16,12)/aug-cc-pVQZ level of theory. The energies are shown in kilojoules per mole. The bond distances (angstroms) and selected bond angles of each molecule are also included. The germanium atoms are colored green, and oxygen atoms are colored red.

We derived the energy-dependent rate constants for the two competing processes, **i1** → **TS1** → **i3** and **i1** → **MSX3** → **p1**, using RRKM theory and assuming that the intersystem crossing is efficient, i.e., treating **MSX3** as a reaction transition state. The results indicate that at an experimental collision energy of 17.5 ± 0.5 kJ mol^{-1}, if the system is to behave statistically, the ratio of the reaction fluxes from **i1** to **i3** and to **p1** through these two pathways should be ∼98/2; this value is actually an underestimate considering that the intersystem crossing is required on the path to **p1**. In view of the experimental observations, this indicates that the reaction dynamics is not only non-adiabatic but also nonstatistical, with the energy likely to be rapidly channeled from the reaction coordinate into the O−O stretching mode. More detailed RRKM calculations would require numerous singlet−triplet crossings and barrierless exit channels to be taken into account where transition states need to be located variationally, but such calculations are still expected to be insufficient for the appropriate description of this reaction because of the apparent nonstatistical behavior. The only theoretical approach that could likely provide an adequate description of this reaction is ab initio molecular dynamics simulation using either pseudoclassical trajectories with surface hopping or wave packet propagation including multiple PESs possibly involved, such as triplet and singlet surfaces correlating to the ground and excited electronic state products GeO + O(^{3}P) and GeO + O(^{1}D). This represents a challenge for a future comprehensive theoretical study.

In conclusion, a merging of the electronic structure calculations and crossed beam experiments propose non-adiabatic reaction dynamics in the germanium (Ge, ^3P_j)−molecular oxygen (O_2, $X^3\Sigma_g^-$) system yields germanium monoxide (GeO, $X^1\Sigma^+$) along with atomic oxygen [**p1**, O(^{3}P)] in its electronic ground state. The reaction is initiated on the singlet surface via barrierless addition of germanium to the oxygen atom leading to a linear singlet (GeOO, **i1**, $C_{\infty v}$, $^1\Sigma^+$) collision complex with ISC from the singlet to the triplet manifold in the exit channel trough **MSX3** terminating the reaction to form germanium monoxide (GeO, $X^1\Sigma^+$) along with atomic oxygen [**p1**, O(^{3}P)] in its electronic ground state. The facile intersystem crossing is likely supported through the "heavy atom effect" of germanium. Due to the heavy atom effect of germanium, intersystem crossing is revealed to be the dominant, if not exclusive, channel for the unimolecular dissociation of **i3** (OGeO, C_{2v}, $^1A_1$) to germanium monoxide (GeO, $X^1\Sigma^+$) and ground state atomic oxygen [**p1**, O(^{3}P)] because the inclusion of heavy atoms in the molecular structure enhances the spin−orbit coupling between singlet and triplet states,[83−86] thus shedding light on the fundamental reaction pathways of the unimolecular decomposition of main group XIV oxides and the inherent formation of subvalent germanium(II) compounds such as germanium monoxide (GeO, $X^1\Sigma^+$).

https://doi.org/10.1021/acs.jpclett.2c00706
J. Phys. Chem. Lett. 2022, 13, 4589−4597

METHODS

Experimental Section. The gas-phase reaction of a germanium (Ge, ^3P_j) atom and oxygen (O_2, $X^3\Sigma_g^-$) with each reactant in its electronic ground state was conducted via single-collision conditions utilizing a homemade universal crossed molecular beam setup.[51] The reactant atomic germanium (Ge, ^3P_j) was generated in the primary source chamber. In brief, the 266 nm laser operated at 30 Hz (Nd:YAG laser, 3 ± 1 mJ per pulse)[82] was used to process *in situ* ablation of germanium atoms from a rotating germanium rod (Alfa Aesar). The neon gas (Ne, 99.999%; Specialty Gases of America) regulated at a backing pressure of 4 atm was utilized to dilute the ablated germanium atoms. No higher-molecular weight germanium-bearing species were observed under the current experimental conditions. The gas mixture was first skimmed and then velocity-selected by a four-slot chopper wheel. A peak velocity (v_p) and speed ratio (S) of the neon-seeded germanium beam were determined to be 982 ± 8 m s^{-1} and 5.9 ± 0.2 (Table S1), respectively. Laser-induced fluorescence interrogation of a neon-seeded germanium beam indicates that all germanium atoms are in their electronic ground state (^3P_j).[82] The relative abundance values for ground states $^3P_0$, $^3P_1$, and $^3P_2$ are derived as 56%, 36%, and 8%, respectively.[87] In the secondary source chamber, pure oxygen gas (O_2, 99.998%; Matheson) was used as precursor to produce the supersonic oxygen beam charactered with a v_p of 778 ± 20 m s^{-1} and an S of 15.6 ± 1.0 (Table S1). In the main chamber, the supersonic oxygen beam interacted with the primary beam germanium atoms at 90°. The resulting collision energy (E_C) is 17.5 ± 0.5 kJ mol^{-1}, while a center of mass angle (Θ_{CM}) is determined to be 18.9° ± 0.6°. The detector, which is a triply differentially pumped and rotatable chamber that can realize the collection of angularly resolved time-of-flight (TOF) spectra in the plane defined by both reactant beams, is located inside of the crossed molecular beam machine. Once entering the detector, the neutral reaction products flew through the electron impact ionizer (80 eV, 2.0 mA),[88] and the resulting ions were then selected via a quadrupole mass spectrometer (QMS, Extrel, QC 150) on the basis of the mass-to-charge ratio. The filtered ions were ultimately collected by a Daly type ion counter.[89] To determine the essence of the reaction dynamics, a forward-convolution method was used to transform the laboratory frame (LAB) data into the center of mass frame (CM) and the CM translational energy $P(E_T)$ and angular $T(\theta)$ flux distributions can be obtained.[90,91] The error ranges of the $P(E_T)$ and $T(\theta)$ functions are determined within the 1σ limits of the corresponding laboratory angular distribution and beam parameters (beam spreads and beam velocities) while maintaining a good fit of the laboratory TOF spectra.

Computational Studies. Geometries of the intermediates and transition states on the GeO_2 PES were initially optimized using the hybrid ωB97XD density functional[92] with Dunning's augmented correlation-consistent aug-cc-pVTZ basis set,[93] and vibrational frequencies were computed at the same ωB97XD/aug-cc-pVTZ level of theory. Then, the structures were reoptimized utilizing the multireference second-order perturbation theory CASPT2 method[94,95] with the augmented quadruple-ζ aug-cc-pVQZ basis set and with full valence active space containing 16 electrons distributed on 12 orbitals. In cases in which a transition state does not exist at the ωB97XD/aug-cc-pVTZ level of theory and could be found only using the CASPT2 method (e.g., for **TS4**), vibrational frequencies were computed numerically at the CASPT2(16,12)/aug-cc-pVQZ level of theory. The minimal energy structures on the seams of crossing (MSX) between singlet and triplet states were located using the multireference complete active space SCF (CASSCF) method[96,97] also with the full valence (16,12) active space and with the x2c-SVPall-2c basis set,[98] and their single-point energies were then improved utilizing CASPT2-(16,12)/aug-cc-pVQZ. Additionally, the energies of the reactants and products were computed at the coupled clusters[99] CCSD(T)/CBS//ωB97XD/aug-cc-pVTZ level with the complete basis set (CBS) extrapolation from the values assessed with the aug-cc-pVQZ and aug-cc-pVTZ basis sets. Potential energy scans carried out to explore the direct O abstraction channel on the triplet PES and to verify barrierless connections between the reactants/products and GeO_2 intermediates were executed at the CASPT2(16,12)/aug-cc-pVQZ level of theory. The electronic structure calculations were performed utilizing Gaussian 09[100] (ωB97XD) and MOLPRO[101] (CASSCF, CASPT2, and the MSX search) software packages.

ASSOCIATED CONTENT

Supporting Information

The Supporting Information is available free of charge at https://pubs.acs.org/doi/10.1021/acs.jpclett.2c00706.

Summary of experimentally determined velocities for each reactant (Table S1) and optimized Cartesian coordinates and vibrational frequencies for each species produced in the Ge(^3P_j)−O_2($X^3\Sigma_g^-$) system (Table S2) (PDF)

AUTHOR INFORMATION

Corresponding Authors

Ralf I. Kaiser − *Department of Chemistry, University of Hawai'i at Mānoa, Honolulu, Hawaii 96822, United States;* orcid.org/0000-0002-7233-7206; Email: ralfk@hawaii.edu

Alexander M. Mebel − *Department of Chemistry and Biochemistry, Florida International University, Miami, Florida 33199, United States;* orcid.org/0000-0002-7233-3133; Email: mebela@fiu.edu

Authors

Chao He − *Department of Chemistry, University of Hawai'i at Mānoa, Honolulu, Hawaii 96822, United States*

Shane J. Goettl − *Department of Chemistry, University of Hawai'i at Mānoa, Honolulu, Hawaii 96822, United States;* orcid.org/0000-0003-1796-5725

Zhenghai Yang − *Department of Chemistry, University of Hawai'i at Mānoa, Honolulu, Hawaii 96822, United States*

Anatoliy A. Nikolayev − *Samara National Research University, Samara 443086, Russia; Lebedev Physical Institute, Samara 443011, Russia*

Valeriy N. Azyazov − *Samara National Research University, Samara 443086, Russia; Lebedev Physical Institute, Samara 443011, Russia*

Complete contact information is available at: https://pubs.acs.org/10.1021/acs.jpclett.2c00706

Notes

The authors declare no competing financial interest.

https://doi.org/10.1021/acs.jpclett.2c00706
J. Phys. Chem. Lett. 2022, 13, 4589−4597

■ ACKNOWLEDGMENTS

The experimental work at the University of Hawai'i at Mānoa was supported by National Science Foundation (NSF) Grant CHE-1853541. The electronic structure calculations at Lebedev Physics Institute were supported by the Ministry of Higher Education and Science of the Russian Federation via Grant 075-15-2021-597.

■ REFERENCES

(1) Winkler, C. Mittheilungen über das Germanium. *J. Prakt. Chem.* **1886**, *34*, 177−229.
(2) Winkler, C. Germanium, Ge, ein neues, nichtmetallisches Element. *Ber. Dtsch. Chem. Ges.* **1886**, *19*, 210−211.
(3) Jutzi, P.; Hoffmann, H. J.; Brauer, D. J.; Krüger, C. Stabilization of Monomeric Dichlorogermylene. *Angew. Chem., Int. Ed.* **1973**, *12*, 1002−1003.
(4) Harris, D. H.; Lappert, M. F. Monomeric, Volatile Bivalent Amides of Group IV_B elements, $M(NR^1_2)_2$ and M $(NR^1R^2)_2$ (M= Ge, Sn, or Pb; R^1=Me_3Si, R^2=Me_3C). *J. Chem. Soc., Chem. Commun.* **1974**, 895−896.
(5) Gynane, M. J. S.; Harris, D. H.; Lappert, M. F.; Power, P. P.; Rivière, P.; Rivière-Baudet, M. Subvalent Group 4B Metal Alkyls and Amides. Part 5. The Synthesis and Physical Properties of Thermally Stable Amides of Germanium(II), Tin(II), and Lead(II). *J. Chem. Soc., Dalton Trans.* **1977**, 2004−2009.
(6) Meller, A.; Gräbe, C. P. Synthese und Isolierung neuer Germanium (II)-Verbindungen und freier Germylene. *Chem. Ber.* **1985**, *118*, 2020−2029.
(7) Meller, A.; Pfeiffer, J.; Noltemeyer, M. Aza-und Thia-2-germa(II)-Indane und entsprechende 2,2′-Spirobi(2-germaindane). *Z. Anorg. Allg. Chem.* **1989**, *572*, 145−150.
(8) Pfeiffer, J.; Maringgele, W.; Noltemeyer, M.; Meller, A. Reaktionen Von Germylenen Mit Aziden: Iminogermane, Azidogermane, Tetrazagermole und Hexaazadigermadispirododecane. *Chem. Ber.* **1989**, *122*, 245−252.
(9) Pineda, L. W.; Jancik, V.; Starke, K.; Oswald, R. B.; Roesky, H. W. Stable Monomeric Germanium(II) and Tin(II) Compounds with Terminal Hydrides. *Angew. Chem.* **2006**, *118*, 2664−2667.
(10) Katir, N.; Matioszek, D.; Ladeira, S.; Escudié, J.; Castel, A. Stable N-Heterocyclic Carbene Complexes of Hypermetallyl Germanium(II) and Tin(II) Compounds. *Angew. Chem., Int. Ed.* **2011**, *50*, 5352−5355.
(11) Nagendran, S.; Roesky, H. W. The Chemistry of Aluminum(I), Silicon(II), and Germanium(II). *Organomet. Chem.* **2008**, *27*, 457−492.
(12) McKellar, A. R. W.; Bunker, P. R.; Sears, T. J.; Evenson, K. M.; Saykally, R. J.; Langhoff, S. R. Far Infrared Laser Magnetic Resonance of Singlet Methylene: Singlet−Triplet Perturbations, Singlet−Triplet Transitions, and the Singlet−Triplet Splitting[a)]. *J. Chem. Phys.* **1983**, *79*, 5251−5264.
(13) Leopold, D. G.; Murray, K. K.; Miller, A. E. S.; Lineberger, W. C. Methylene: A Study of the X^3B_1 and a^1A_1 States by Photoelectron Spectroscopy of CH^-_2 and CD^-_2. *J. Chem. Phys.* **1985**, *83*, 4849−4865.
(14) Colvin, M. E.; Grev, R. S.; Schaefer, H. F., III; Bicerano, J. $\tilde{X}^1A_1$, $\tilde{a}^3B_1$, and $\tilde{A}^1B_1$ Electronic State of Silylenes. Structures and Vibrational Frequencies of SiH_2, and SiHF, and SiF_2. *Chem. Phys. Lett.* **1983**, *99*, 399−405.
(15) Rice, J. E.; Handy, N. C. The Low-Lying States of Silylene. *Chem. Phys. Lett.* **1984**, *107*, 365−374.
(16) Gordon, M. S. Potential-Energy Surfaces in Singlet and Triplet Silylene. *Chem. Phys. Lett.* **1985**, *114*, 348−352.
(17) Balasubramanian, K.; McLean, A. D. The Singlet−Triplet Energy Separation in Silylene. *J. Chem. Phys.* **1986**, *85*, 5117−5119.
(18) Gordon, M. S.; Gano, D. R.; Binkley, J. S.; Frisch, M. J. Thermal Decomposition of Silane. *J. Am. Chem. Soc.* **1986**, *108*, 2191−2195.
(19) Koseki, S.; Gordon, M. S. Potential Energy Surfaces and Dynamical Properties of Three Low-Lying States of Silylene. *J. Mol. Spectrosc.* **1987**, *123*, 392−404.
(20) Selmani, A.; Salahub, D. R. On the Singlet−Triplet Splitting in SiH_2, GeH_2, and SnH_2. Local-Spin-Density Calculations. *J. Chem. Phys.* **1988**, *89*, 1529−1532.
(21) Matsunaga, N.; Koseki, S.; Gordon, M. S. Relativistic Potential Energy Surfaces of XH_2 (X = C, Si, Ge, Sn, and Pb) Molecules: Coupling of $^1A_1$ and $^3B_1$ States. *J. Chem. Phys.* **1996**, *104*, 7988−7996.
(22) Gaspar, P. P.; Xiao, M.; Pae, D. H.; Berger, D. J.; Haile, T.; Chen, T.; Lei, D.; Winchester, W. R.; Jiang, P. The Quest for Triplet Ground State Silylenes. *J. Organomet. Chem.* **2002**, *646*, 68−79.
(23) Barrau, J.; Rima, G. Stable Sermanium Analogs of Carbenes, Imines, Ketones, Thiones, Selones and Tellones. *Coord. Chem. Rev.* **1998**, *178*, 593−622.
(24) Regitz, M. Stable Carbenes—Illusion or Reality? *Angew. Chem., Int. Ed.* **1991**, *30*, 674−676.
(25) Herrmann, W. A.; Köcher, C. N-Heterocyclic Carbenes. *Angew. Chem., Int. Ed.* **1997**, *36*, 2162−2187.
(26) Arduengo, A. J., III; Harlow, R. L.; Kline, M. A Stable Crystalline Carbene. *J. Am. Chem. Soc.* **1991**, *113*, 361−363.
(27) Bourissou, D.; Guerret, O.; Gabbai, F. P.; Bertrand, G. Stable Carbenes. *Chem. Rev.* **2000**, *100*, 39−92.
(28) Nair, V.; Bindu, S.; Sreekumar, V. N-Heterocyclic Carbenes: Reagents, Not Just Ligands. *Angew. Chem., Int. Ed.* **2004**, *43*, 5130−5135.
(29) Weidenbruch, M. Some Silicon, Germanium, Tin, and Lead Analogues of Carbenes, Alkenes, and Dienes. *Eur. J. Inorg. Chem.* **1999**, *1999*, 373−381.
(30) Gehrhus, B.; Lappert, M. F. Chemistry of Thermally Stable Bis(amino) Silylenes. *J. Organomet. Chem.* **2001**, *617*, 209−223.
(31) Kira, M. Isolable Silylene, Disilenes, Trisilaallene, and Related Compounds. *J. Organomet. Chem.* **2004**, *689*, 4475−4488.
(32) Gilliam, O. R.; Johnson, C. M.; Gordy, W. Microwave Spectroscopy in the Region from Two to Three Millimeters. *Phys. Rev.* **1950**, *78*, 140.
(33) Lide, D. R.; Haynes, W. M. *CRC handbook of chemistry and physics*; CRC Press: Boca Raton, FL, 2010; Vol. *9*.
(34) Mabery, C. F. The Composition of Certain Products from the Cowles Electrical Furnace. *J. Franklin Inst.* **1887**, *9*, 11−15.
(35) Mellor, J. W. *Mellor's Comprehensive Treatise on Inorganic and Theoretical Chemistry*; John Wiley & Sons: New York, 1972.
(36) Hohl, A.; Wieder, T.; Van Aken, P. A.; Weirich, T. E.; Denninger, G.; Vidal, M.; Oswald, S.; Deneke, C.; Mayer, J.; Fuess, H. An Interface Clusters Mixture Model for the Structure of Amorphous Silicon Monoxide (SiO). *J. Non-Cryst. Solids* **2003**, *320*, 255−280.
(37) Bernstein, L. R. Germanium Ggeochemistry and Mmineralogy. *Geochim. Cosmochim. Acta* **1985**, *49*, 2409−2422.
(38) Vega, F.; Afonso, C. N.; Solis, J. Real Time Emission Spectroscopy During Deposition of Germanium Oxide Films by Laser Ablation. *Appl. Surf. Sci.* **1993**, *69*, 403−406.
(39) Prabhakaran, K.; Nishioka, T.; Sumitomo, K.; Kobayashi, Y.; Ogino, T. In Situ Oxidation of a Thin Layer of Ge on Si(001): Observation of GeO to SiO_2 Transition. *Appl. Phys. Lett.* **1993**, *62*, 864−866.
(40) Lee, E. G.; Seto, J. Y.; Hirao, T.; Bernath, P. F.; Le Roy, R. J. FTIR Emission Spectra, Molecular Constants, and Potential Curve of Ground State GeO. *J. Mol. Spectrosc.* **1999**, *194*, 197−202.
(41) Baig, M. A.; Connerade, J. P. Rydberg States of the GeO Molecule. *J. Mol. Spectrosc.* **1980**, *83*, 31−39.
(42) Appelblad, O.; Fredin, S.; Lagerqvist, A.; Alberti, F. The Spectra of $^{74}Ge^{16}O$ and $^{74}Ge^{18}O$ in the Vacuum Ultraviolet Region. *Phys. Scr.* **1983**, *28*, 160−170.
(43) Hormes, J.; Petersen, S.; Scullman, R. The Ultraviolet Absorption Spectra of GeO in Rare Gas Matrices. *J. Mol. Spectrosc.* **1985**, *110*, 141−152.
(44) Mummigatti, V. M.; Jyoti, B. G. RKRV Franck—Condon Factors and r-Centroids for the $(A^1\Pi - X^1\Sigma^+)$ transition of GeO

https://doi.org/10.1021/acs.jpclett.2c00706
J. Phys. Chem. Lett. 2022, 13, 4589−4597

molecule. *Acta Physica Academiae Scientiarum Hungaricae* **1977**, *42*, 99−102.
(45) Sefyani, F. L.; Schamps, J.; Duflot, D. Theoretical Study of the Radiative Properties of the $A^1\Pi$-$X^1\Sigma^+$ system of the GeO molecule. *J. Quant. Spectrosc. Radiat. Transfer* **1995**, *54*, 1027−1034.
(46) Kellö, V.; Sadlej, A. J. The Nuclear Quadrupole Moment of ^{73}Ge from Molecular Microwave Data. *Mol. Phys.* **1999**, *96*, 275−281.
(47) Jevons, W.; Bashford, L. A.; Briscoe, H. V. A. The Ultra-Violet Band-System of Germanium Monoxide. *Proceedings of the Physical Society* **1937**, *49*, 543.
(48) Barrow, R. F.; Rowlinson, H. C. The Absorption Spectra of the Gaseous Monoxides of Silicon, Germanium and Tin in the Schumann Region. *Proc. R. Soc. A* **1954**, *224*, 374−388.
(49) Rowlinson, H. C.; Barrow, R. F. Absorption Band Systems of SiO and GeO in the Schumann Region. *J. Chem. Phys.* **1953**, *21*, 378−379.
(50) Colbourn, E. A.; Dyke, J. M.; Fackerell, A.; Morris, A.; Trickle, I. R. Vacuum Ultraviolet Photoelectron Spectrum of the GeO($X^1\Sigma^+$) Molecule. *J. Chem. Soc., Faraday Trans.* **1978**, *74*, 2278−2285.
(51) Kaiser, R. I.; Maksyutenko, P.; Ennis, C.; Zhang, F.; Gu, X.; Krishtal, S. P.; Mebel, A. M.; Kostko, O.; Ahmed, M. Untangling the Chemical Evolution of Titan's Atmosphere and Surface−from Homogeneous to Heterogeneous Chemistry. *Faraday Discuss.* **2010**, *147*, 429−478.
(52) Kaiser, R. I.; Parker, D. S. N.; Mebel, A. M. Reaction Dynamics in Astrochemistry: Low-Temperature Pathways to Polycyclic Aromatic Hydrocarbons in the Interstellar Medium. *Annu. Rev. Phys. Chem.* **2015**, *66*, 43−67.
(53) Yuan, D.; Yu, S.; Chen, W.; Sang, J.; Luo, C.; Wang, T.; Xu, X.; Casavecchia, P.; Wang, X.; Sun, Z.; et al. Direct Observation of Forward-Scattering Oscillations in the H+HD→H_2+D Reaction. *Nat. Chem.* **2018**, *10*, 653−658.
(54) Yuan, D.; Chen, W.; Luo, C.; Tan, Y.; Li, S.; Huang, Y.; Sun, Z.; Yang, X.; Wang, X. Imaging the State-to-State Dynamics of the H + D_2→ HD+ D Reaction at 1.42 eV. *J. Phys. Chem. Lett.* **2020**, *11*, 1222−1227.
(55) Yuan, D.; Huang, Y.; Chen, W.; Zhao, H.; Yu, S.; Luo, C.; Tan, Y.; Wang, S.; Wang, X.; Sun, Z.; Yang, X. Observation of the Geometric Phase Effect in the H+HD→H_2+D Reaction Below the Conical Intersection. *Nat. Commun.* **2020**, *11* (1−7), 3640.
(56) Balucani, N.; Skouteris, D.; Capozza, G.; Segoloni, E.; Casavecchia, P.; Alexander, M. H.; Capecchi, G.; Werner, H.-J. The Dynamics of the Prototype Abstraction Reaction Cl($^2P_{3/2,1/2}$) + H_2: A Comparison of Crossed Molecular Beam Experiments with Exact Quantum Scattering Calculations on Coupled ab Initio Potential Energy Surfaces. *Phys. Chem. Chem. Phys.* **2004**, *6*, 5007−5017.
(57) Skouteris, D.; Werner, H.-J.; Aoiz, F. J.; Banares, L.; Castillo, J. F.; Menéndez, M.; Balucani, N.; Cartechini, L.; Casavecchia, P. Experimental and Theoretical Differential Cross Sections for the Reactions Cl + H_2/D_2. *J. Chem. Phys.* **2001**, *114*, 10662−10672.
(58) Yang, T.; Chen, J.; Huang, L.; Wang, T.; Xiao, C.; Sun, Z.; Dai, D.; Yang, X.; Zhang, D. H. Extremely Short-Lived Reaction Resonances in Cl + HD (v = 1)→ DCl + H due to Chemical Bond Softening. *Science* **2015**, *347*, 60−63.
(59) Xie, Y.; Wang, Y.; Wang, W.; Dai, D.; Sun, Z.; Xiao, C.; Yang, X. Experimental and Theoretical Study of the Vibrationally Excited Reaction Cl + D_2 (v = 1, j = 0) → DCl + D. *J. Phys. Chem. A* **2020**, *124*, 1266−1271.
(60) Xie, Y.-r.; Wang, Y.-f.; Wang, W.; Wang, T.; Dai, D.-x.; Xiao, C.-l.; Yang, X.-m. Crossed Beam Experiment on the Validity of Born-Oppenheimer Approximation in Cl(^{2}P)+D_2→DCl+D Reaction. *Chin. J. Chem. Phys.* **2020**, *33*, 135−138.
(61) Lee, S.-H.; Dong, F.; Liu, K. A Crossed-Beam Study of the F + HD→ HF + D Reaction: The Resonance-Mediated Channel. *J. Chem. Phys.* **2006**, *125*, 133106.
(62) Wang, T.; Chen, J.; Yang, T.; Xiao, C.; Sun, Z.; Huang, L.; Dai, D.; Yang, X.; Zhang, D. H. Dynamical Resonances Accessible only by Reagent Vibrational Excitation in the F + HD→HF+ D Reaction. *Science* **2013**, *342*, 1499−1502.
(63) Yang, T.; Huang, L.; Wang, T.; Xiao, C.; Xie, Y.; Sun, Z.; Dai, D.; Chen, M.; Zhang, D.; Yang, X. Effect of Reagent Vibrational Excitation on the Dynamics of F + H_2(v = 1, j = 0) → HF (v', j') + H Reaction. *J. Phys. Chem. A* **2015**, *119*, 12284−12290.
(64) Yang, T.-g.; Huang, L.; Xie, Y.-r.; Wang, T.; Xiao, C.-l.; Sun, Z.-g.; Dai, D.-x.; Chen, M.-d.; Zhang, D. H.; Yang, X.-m. Effect of Reagent Rotational Excitation on Dynamics of F+H_2→HF+H. *Chin. J. Chem. Phys.* **2015**, *28*, 471.
(65) Huang, L.; Xie, Y.-r.; Yang, T.-g.; Wang, T.; Dai, D.-x.; Xiao, C.-l.; Yang, X.-m. Crossed Molecular Beam Study of the F+D_2(v = 1, j = 0) Reaction. *Chin. J. Chem. Phys.* **2019**, *32*, 72−76.
(66) Balucani, N.; Casavecchia, P.; Aoiz, F.; Bañares, L.; Launay, J.-M.; Bussery-Honvault, B.; Honvault, P. Dynamics of the C(^{1}D)+H_2 Reaction: A Comparison of Crossed Molecular Beam Experiments with Quantum Mechanical and Quasiclassical Trajectory Calculations on the First Two Singlet (1^1A′ and 1^1A″) Potential Energy Surfaces. *Mol. Phys.* **2010**, *108*, 373−380.
(67) Balucani, N.; Capozza, G.; Segoloni, E.; Russo, A.; Bobbenkamp, R.; Casavecchia, P.; Gonzalez-Lezana, T.; Rackham, E. J.; Bañares, L.; Aoiz, F. J. Dynamics of the C(^1D) + D_2 Reaction: A Comparison of Crossed Molecular-Beam Experiments with Quasi-classical Trajectory and Accurate Statistical Calculations. *J. Chem. Phys.* **2005**, *122*, 234309.
(68) Pederson, L. A.; Schatz, G. C.; Ho, T.-S.; Hollebeek, T.; Rabitz, H.; Harding, L. B.; Lendvay, G. Potential Energy Surface and Quasiclassical Trajectory Studies of the N(^{2}D)+H_2 Reaction. *J. Chem. Phys.* **1999**, *110*, 9091−9100.
(69) Balucani, N.; Alagia, M.; Cartechini, L.; Casavecchia, P.; Volpi, G. G.; Pederson, L. A.; Schatz, G. C. Dynamics of the N(^{2}D) + D_2 Reaction from Crossed-Beam and Quasiclassical Trajectory Studies. *J. Phys. Chem. A* **2001**, *105*, 2414−2422.
(70) Balucani, N.; Cartechini, L.; Capozza, G.; Segoloni, E.; Casavecchia, P.; Volpi, G. G.; Javier Aoiz, F.; Bañares, L.; Honvault, P.; Launay, J.-M. Quantum Effects in the Differential Cross Sections for the Insertion Reaction $N(^2D)$ + H_2. *Phys. Rev. Lett.* **2002**, *89*, 013201.
(71) Balucani, N.; Casavecchia, P.; Banares, L.; Aoiz, F. J.; Gonzalez-Lezana, T.; Honvault, P.; Launay, J.-M. Experimental and Theoretical Differential Cross Sections for the N(^{2}D) + H_2 Reaction. *J. Phys. Chem. A* **2006**, *110*, 817−829.
(72) Liu, X.; Lin, J. J.; Harich, S.; Schatz, G. C.; Yang, X. A Quantum State-Resolved Insertion Reaction: O(^{1}D)+ H_2(J = 0) → OH($^2\prod$, v, N) + H(^{2}S). *Science* **2000**, *289*, 1536−1538.
(73) Balucani, N.; Casavecchia, P.; Aoiz, F. J.; Banares, L.; Castillo, J. F.; Herrero, V. J. Dynamics of the O(1D) D2 Reaction: A Comparison Between Crossed Molecular Beam Experiments and Quasiclassical Trajectory Calculations on the Lowest Three Potential Energy Surfaces. *Mol. Phys.* **2005**, *103*, 1703−1714.
(74) Lee, S.-H.; Liu, K. Direct Mapping of Insertion Reaction Dynamics: S(^{1}D)+H_2→SH+H. *Appl. Phys. B: Laser Opt.* **2000**, *71*, 627−633.
(75) Maiti, B.; Schatz, G. C.; Lendvay, G. Importance of Intersystem Crossing in the S(^{3}P, ^{1}D) + H_2 → SH + H Reaction. *J. Phys. Chem. A* **2004**, *108*, 8772−8781.
(76) Yang, H.; Han, K.-L.; Schatz, G. C.; Lee, S.-H.; Liu, K.; Smith, S. C.; Hankel, M. Integral and Differential Cross Sections for the S(^1D)+HD Reaction Employing the Ground Adiabatic Electronic State. *Phys. Chem. Chem. Phys.* **2009**, *11*, 11587−11595.
(77) Levine, R. D. *Molecular Reaction Dynamics*; Cambridge University Press: Cambridge, U.K., 2005.
(78) Miller, W. B.; Safron, S. A.; Herschbach, D. R. Exchange Reactions of Alkali Atoms with Alkali Halides: a Collision Complex Mechanism. *Discuss. Faraday Soc.* **1967**, *44*, 108−122.
(79) Ribeiro, J. M.; Mebel, A. M. Reaction Mechanism and Product Branching Ratios of the CH + C_3H_4 Reactions: A Theoretical Study. *Phys. Chem. Chem. Phys.* **2017**, *19*, 14543−14554.
(80) Doering, J. P.; Gulcicek, E. E. Absolute Differential and Integral Electron Excitation Cross Sections for Atomic Oxygen 7. The ^{3}P →

https://doi.org/10.1021/acs.jpclett.2c00706
J. Phys. Chem. Lett. 2022, 13, 4589−4597

^{1}D and ^{3}P → ^{1}S transitions from 4.0 to 30 eV. *J. Geophys. Res. A: Space Phys.* **1989**, *94*, 1541−1546.
(81) Rau, H.; Schnedler, E. Standard Molar Enthalpy of Formation of GeO(g) from Flow Measurements. *J. Chem. Thermodynamics* **1984**, *16*, 673−682.
(82) Thomas, A. M.; Dangi, B. B.; Yang, T.; Tarczay, G. r.; Kaiser, R. I.; Sun, B.-J.; Chen, S.-Y.; Chang, A. H. H.; Nguyen, T. L.; Stanton, J. F.; Mebel, A. M. Directed Gas-Phase Formation of the Germaniumsilylene Butterfly Molecule (Ge(μ-H_2)Si). *J. Phys. Chem. Lett.* **2019**, *10*, 1264−1271.
(83) Koziar, J. C.; Cowan, D. O. Photochemical Heavy-atom Effects. *Acc. Chem. Res.* **1978**, *11*, 334−341.
(84) Alagia, M.; Balucani, N.; Cartechini, L.; Casavecchia, P.; van Beek, M.; Gualberto Volpi, G.; Bonnet, L.; Claude Rayez, J. Crossed Beam Studies of the O(^{3}P, ^{1}D)+CH_3I Reactions: Direct Evidence of Intersystem Crossing. *Faraday Discuss.* **1999**, *113*, 133−150.
(85) Hwang, D.-Y.; Mebel, A. M. Ab Initio Study of Spin-forbidden Unimolecular Decomposition of Carbon Dioxide. *Chem. Phys.* **2000**, *256*, 169−176.
(86) Geppert, W. D.; Naulin, C.; Costes, M. Integral Cross-section of the C(^3P_J)+O_2($X^3\Sigma_g^-$)→CO($X^1\Sigma^+$)+O($^1D_2$) Reaction between 0.41 and 12.0 kJ/mol. *Chem. Phys. Lett.* **2002**, *364*, 121−126.
(87) Herzberg, G.; Mrozowski, S. Molecular Spectra and Molecular Structure. I. Spectra of Diatomic Molecules. *American Journal of Physics* **1951**, *19*, 390−391.
(88) Brink, G. O. Electron Bombardment Molecular Beam Detector. *Rev. Sci. Instrum.* **1966**, *37*, 857−860.
(89) Daly, N. R. Scintillation Type Mass Spectrometer Ion Detector. *Rev. Sci. Instrum.* **1960**, *31*, 264−267.
(90) Weiss, P. S. The Reactions of Ground and Excited Dtate Sodium Atoms with Hydrogen Halide Molecules. Ph.D. Dissertation, University of California, Berkeley, CA, 1986.
(91) Vernon, M. F. Molecular Beam Scattering. Ph.D. Dissertation, University of California, Berkeley, CA, 1983.
(92) Chai, J.-D.; Head-Gordon, M. Long-Range Corrected Hybrid Density Functionals with Damped Atom−Atom Dispersion Corrections. *Phys. Chem. Chem. Phys.* **2008**, *10*, 6615−6620.
(93) Dunning, T. H., Jr Gaussian Basis Sets for Use in Correlated Molecular Calculations. I. the Atoms Boron through Neon and Hydrogen. *J. Chem. Phys.* **1989**, *90*, 1007−1023.
(94) Celani, P.; Werner, H.-J. Multireference perturbation theory for large restricted and selected active space reference wave functions. *J. Chem. Phys.* **2000**, *112*, 5546−5557.
(95) Shiozaki, T.; Győrffy, W.; Celani, P.; Werner, H.-J. Communication: extended multi-state complete active space second-order perturbation theory: energy and nuclear gradients. *J. Chem. Phys.* **2011**, *135*, 081106.
(96) Werner, H. J.; Knowles, P. J. A Second Order Multiconfiguration SCF Procedure with Optimum Convergence. *J. Chem. Phys.* **1985**, *82*, 5053−5063.
(97) Knowles, P. J.; Werner, H.-J. An Efficient Second-order MC SCF Method for Long Configuration Expansions. *Chem. Phys. Lett.* **1985**, *115*, 259−267.
(98) Pollak, P.; Weigend, F. Segmented Contracted Error-Consistent Basis Sets of Double-and Triple-ζ Valence Quality for One-and Two-Component Relativistic All-Electron Calculations. *J. Chem. Theory Comput.* **2017**, *13*, 3696−3705.
(99) Purvis, G. D., III; Bartlett, R. J. A Full Coupled-Cluster Singles and Doubles Model: The Inclusion of Disconnected Triples. *J. Chem. Phys.* **1982**, *76*, 1910−1918.
(100) Frisch, M. J.; Trucks, G. W.; Schlegel, H. B.; Scuseria, G. E.; Robb, M. A.; Cheeseman, J. R.; Scalmani, G.; Barone, V.; Mennucci, B.; Petersson, G. A.; et al. *Gaussian 16*, rev. C.1; Gaussian, Inc.: Wallingford, CT, 2019.
(101) Werner, H.-J.; Knowles, P. J.; Knizia, G.; Manby, F. R.; Schütz, M.; Celani, P.; Györffy, W.; Kats, D.; Korona, T.; Lindh, R.; et al. *MOLPRO*, ver. 2021.2; University of Cardiff: Cardiff, U.K., 2021 (http://www.molpro.net).

https://doi.org/10.1021/acs.jpclett.2c00706
J. Phys. Chem. Lett. 2022, 13, 4589−4597